This is the Pre-Published Version.
The following publication Li, Y., Lin, S., San Chui, Y., & Lau, S. P. (2016). Effect of uniaxial strain on low frequency Raman modes in few layers molybdenum disulfide. ECS Journal of Solid State Science and Technology, 5(11), Q3033 is available at https://doi.org/10.1149/2.0071611jss.

Effect of Uniaxial Strain on Low Frequency Raman Modes in Few Layers Molybdenum Disulfide

Yanyong Li, Shenghuang Lin, Ying San Chui, and Shu Ping Lau*

Department of Applied Physics, The Hong Kong Polytechnic University, Hong Kong SAR, China

The effect of uniaxial tensile strain on the shear mode (C mode) and layer breathing mode (LB mode) of few layers MoS_2 were studied. The C mode is doubly degenerated into two sub-peaks as applied strain increases. No measurable Raman shift for the LB mode is observed, while its Raman intensity decreases gradually as the strain increases. In addition, the C and LB modes exhibit distinguished thickness dependence. The C mode shows a clear blue shift as the strain increases, while the LB mode is softened in the process. Moreover, the evolution of C mode with thickness follows an enhanced linear-chain model plus a linear component very well. It implies that the C mode is a better thickness navigator as compared to the L mode.

Molybdenum disulfide (MoS_2) is a kind of typical transition metal dichalcogenide semiconductor with an indirect bandgap of 1.29 eV. [1] In recent years, atomically thick MoS_2 layers have been fabricated by direct mechanical exfoliation[2] and chemical vapor deposition[3]. Few layers MoS_2 films have attracted lots of attention because of its intriguing electronic and optical properties. For instance, the room temperature current on/off ratio of monolayer MoS_2 transistor can reach 10^8, which is much larger than devices based on graphene.[4] In addition, excellent photoluminescence is revealed in MoS_2 layers resulting from *d*-orbital related interaction.[5] Monolayer MoS_2 serving as an inverter in a logical circuit with a larger gain factor than conventional semiconductors.[6, 7] These fantastic properties of MoS_2 are results from its intrinsic band structure. Bulk MoS_2 is composed of weakly interacting layers by van der Waals' (vdWs) force with a monolayer thickness of 0.65 nm.[8] In each layer, S-Mo-S covalent bonds

* Corresponding author: apsplau@polyu.edu.hk

This manuscript version is made available under the CC-BY-NC-ND 4.0 license http://creativecommons.org/licenses/by-nc-nd/4.0/

constitute a stable unit, which forms two hexagonal planes of S atoms. An intermediate hexagonal plane of Mo atoms is coordinated through ionic-covalent interaction with the S atoms in a trigonal prismatic arrangement as shown in Figure 1a. As the thickness decreases, MoS_2 undergoes a transition from indirect to a direct bandgap of 1.9 eV in monolayer. [1, 5, 9] Moreover, the bandgap of few layers MoS_2 not only depends on its intrinsic thickness but also the external conditions, such as strain. Strain engineering is a powerful tool to modify the properties of materials, especially for ultrathin materials, which can be used to increase carrier mobility and enhance emission efficiency. Graphene under about 1% tensile strain possesses a band gap opening of 300 meV.[10] Since the few layers MoS_2 is highly elastic and robust, it can easily be strained to modulate its properties. For example, the tensile strain can lead to a transition from direct to indirect bandgap in atomically thick MoS_2 when the strain is up to 1%, while the compressive strain will widen the direct bandgap.[11-13] Particularly, the mechanism of the strain induced properties results from the distortion of the crystal lattice of 2D materials. Since lots of works have studied the effect of phonon vibration in high frequency in few layer MoS_2 by Raman spectroscopy,[14-18] the strain dependence of phonon vibration modes in low frequency range has seldom been studied as the Rayleigh line is strong and broad to hinder the fine Raman modes in low frequency. The high frequency modes normally are corresponding to the vibration in intralayer chemical bonds and are stronger than the low frequency ones. In contrast, the low frequency modes result from the vdWs force induced weak layer-layer vibrations with each layer as a whole. Therefore, the low frequency modes are more sensitive to the interlayer coupling and thickness, which has been studied in graphene widely.[19] Herein, we study the evolution of low frequency Raman modes, i.e. the shear (C mode) and layer breathing modes (LB modes) in few layers MoS_2 under controllable uniaxial strain. It is found that the C mode can split into two sub-peaks as the uniaxial strain rises up like the behavior of the high frequency E_{2g}^1 mode. Most importantly, the strain induced two sub-peaks show opposite Raman shifts.

In addition, the C and LB modes are more sensitive than the high frequency modes implying the low frequency modes are better to act as a pointer to the layer number in MoS_2.

Experimental

Sample fabrication- Few layers MoS_2 flakes were mechanical exfoliated onto clean silicon wafer (285 nm SiO_2) by Scotch tape from bulk MoS_2 crystal (SPI Supplies). After identification, the MoS_2 flakes were transferred onto a PET substrate (121 μm thick) with an area of 24 mm × 20 mm using Polydimethylsiloxane (PDMS) film (from Gel-Pak).[20] The flexible PET substrate was able to provide controllable uniaxial strain if bended with various curvatures.[21] Before the transfer of few layers MoS_2 flakes, a layer of SU-8 photoresist (~400 nm) was pre-coated on the PET substrate to raise the visibility of the MoS_2 and reducing the surface roughness of the substrate, which can ensure a good adhesion of the MoS_2 flakes on the PET substrate.[22] The MoS_2 flakes were deposited at the center of the PET substrate as far as possible. As the size of the MoS_2 flakes were much smaller than the thickness of the substrate, the induced strain to the MoS_2 can be assumed to be the same as the strain applied to the PET substrate.[22] Finally, a ~100 nm thick poly(methyl methacrylate) (PMMA) layer was spin coated onto the MoS_2 flake to prevent the slippage between the sample and the substrate.[23-25]

Atomic force microscope- Veeco Multimode 8 was used to determine the thickness of the MoS_2 flakes on silicon wafer in tapping mode. The scanning area was ~10 μm^2 to ensure the AFM image resolution.

Ultralow frequency Raman spectroscopy- Raman spectroscopy measurement was conducted on Horiba HR800 Raman spectroscopy system. An external diode pumped solid state laser of 488 nm was utilized to excite the sample in the confocal Raman system. A neutral filter was used to attenuate the laser power down to 15 μW on the MoS_2 flakes in order to avoid sample heating. As the effect from Rayleigh line, the ultralow frequency module was employed in the Raman system in order to obtain the modes with

frequency lower than 10 cm^{-1}, including three BragGrate notch filters. We used a 100X objective to make the laser spot size of 1 μm. A 1800 graves/mm grating was chosen to enable a spectral resolution of ~ 0.6 cm^{-1} at 488 nm.

Results and discussion

There are four first-order Raman active modes in bulk 2H-MoS_2 because of the D_{6h} space group, E_{2g}^1 mode (383 cm^{-1}), A_{1g} mode (408 cm^{-1}), E_{2g}^2 mode (32cm^{-1}) and E_{1g} mode (286 cm^{-1}).[26, 27] As shown in Figure 1b, the E_{2g}^1 mode is in-plane optical opposite vibration of sulfur atoms and molybdenum atoms against each layer. The A_{1g} mode is assigned as the out of plane optical vibration of sulfur atoms in opposite directions. The E_{2g}^2 mode is also known as the shear mode deriving from the rigid in-plane atomic vibration against neighbor layers. The wavenumber of E_{2g}^2 mode is often lower than 50 cm^{-1} covered by the strong Rayleigh line, which can be rejected under ultralow frequency measurement set up. As for the E_{1g} mode, it is associated with the in-plane opposite vibration of sulfur atoms. However, under backscattering configuration, E_{1g} mode is negligible due to the forbidden selection rule based on the lattice symmetry.[27]

The evolution of normal and ultralow frequency Raman modes dependent on the thickness in various MoS_2 flakes are shown in Figure 2a and 2b respectively. For samples from 3-layer to bulk, a clear red shift (~ 0.7 cm^{-1}) of E_{2g}^1 mode is observed, but the A_{1g} mode gives an apparent blue shit from 405.7 cm^{-1} in the 3-layer flake to 408.2 cm^{-1} in the bulk. Normally, as the layer increases, the internal interaction resulting from the vdWs force will become strong and lead to the phonon mode hardening.[28] In A_{1g} mode, the phonon vibrates along the out of plane direction so that strong vdWs interaction results in the stiffness of lattice vibration, which agrees with the previous studies.[29] However, the opposite trend of E_{2g}^1 mode can attribute to the influence of stacking induced lattice deformation or long range Coulombic interlayer interaction.[30] The C mode is directly relative to the thickness of MoS_2 flake because they are

directly related to the rigid displacement of the layer themselves. Similarly, the C mode also exhibits thickness dependence. As the layer number (N) increases, the C mode reveals a clear blue shift from 22.6 cm^{-1} in the 3-layer sample to 32.4 cm^{-1} in the bulk as shown in Figure 2b. It illustrates that the internal layer interaction make the E_{2g}^{2} mode stiffen gradually, which implies that the C mode can be utilized to monitor the thickness of MoS_2. In addition, a broad flat peak centered at 38.3 cm^{-1} is observed in the 3-layer MoS_2 flake and it gradually shifts toward the low wavenumber as the layer increases as shown in Figure 2b (guided by the red dot arrow lines). Moreover, the peak cannot be observed in bulk. Based on the evolution dependent on the thickness of the MoS_2, this broad flat peak can be assigned as the layer breath mode (LB mode).[31-33] The LB mode represents the rigid layer vibrates perpendicular to the atomic planes, which results from the weakness of the interlayer bonding. Considering the C mode is doubly degenerated, the intensity of C mode should be twice stronger than that of the LB mode meaning that the LB mode is much weaker than the C mode, which has been evident from our results as shown in Figure 2b.

The peak position shifts of the two high frequency Raman modes as a function of 1/N are plotted in Figure 2c. The variations of Raman shift for A_{1g} mode is 2.5 cm^{-1} is much larger than that of E_{2g}^{1} mode meaning that A_{1g} mode is more sensitive to the N. The difference of Raman shifts (Δω) for the two modes is often used as a pointer to the sample thickness. The Δω as a function of 1/N is fitted by a linear function with a slope of -9.69 cm^{-1}/N^{-1} as shown in the inset of Figure 2c.

The rigid layer modes exist in layered crystal where strong and weak forces coexist. They are directly related to the intralayer vdWs forces. The relationship between the C mode and N in graphene has been illustrated by a linear- chain model,[19]

$$\omega = \frac{1}{\sqrt{2}\pi c}\sqrt{\frac{\alpha}{\mu}}\sqrt{1+\cos(\frac{\pi}{N})} \quad (1)$$

where c is the speed of light ($3.0 \times 10^{10}\ cm/s$), μ is the unit layer mass per unit area, and α is the interlayer force constant per unit area. Here, the relationship is also used to illustrate the evolution of C mode in few layers MoS_2. As shown in Figure 2d, the peak position of C mode is extracted from the flakes as a function of the reciprocal of N. The solid dot points for a given thickness derive from the experiment results from different MoS_2 samples. The red dash dot line is the fitting curve using equation (1). The value of $\frac{\alpha}{\mu}$ is $1.69 \times 10^6\ s^{-2}$. However, the fitting is not satisfactory as lots of experimental points deviate from the fitting line. In Ref. 21, graphene is free-suspended on 2~5 μm holes so that no interaction between the bottom and the substrate is considered into the fitting. However, our few layers MoS_2 flakes were deposited onto PET substrate. Weak vdWs interaction must exist between the MoS_2 and PET substrate. As the hardening of C mode is due to an increase of the overall restoring force, the weak vdWs force between MoS_2 and substrate also should be taken into consideration which acts as an additional spring constant in the linear chain model. In order to fit the experimental data better, a modified linear chain model is used by adding a linear component, $k \times \frac{1}{N}$, as follows,

$$\omega = \frac{1}{\sqrt{2}\pi c}\sqrt{\frac{\alpha}{\mu}}\sqrt{1+\cos(\frac{\pi}{N})} + k\frac{1}{N} \qquad (2)$$

The fitting curve is given by the blue dash dot line as shown in Figure 2d. It is found that the fitting using equation 2 is much better than that of equation 1. The fitting parameters $\frac{\alpha}{\mu}$ and k are 1.75×10^6 and -13.4 cm^{-1} respectively, which are similar to the values obtained by equation 1. It implies that the linear-chain model part is almost the same and that the additional linear component is ascribed to the weak vdWs interaction between the MoS_2 flake and the PET substrate.

Figure 3a shows the optical image of the MoS_2 flakes deposited on the PET substrate. The laser spot is mainly focused on the area highlighted by the red dashed circle. After all the experiments, the thickness of this flake was determined as 8.71 nm by atomic force microscope as shown in the inset of Figure 3b. The morphology of the MoS_2 flake is quite flat with clear edges. The strain was applied to

the MoS_2 flake by bending the substrate (Figure 1c).[14, 34-36] The uniaxial strain (ε) is applied along the bending direction as indicated by the green arrows. The strain was calculated based on the formula, $\varepsilon = \frac{d}{2r}$ where d is the thickness of the substrate and r is the radius of curvature of the bended substrate as shown in the inset of Figure 1c.

The E_{2g}^1 and A_{1g} modes of the unstrained MoS_2 are centered at 383.3 cm^{-1} and 406.7 cm^{-1} respectively. As the strain rises up gradually, the A_{1g} mode maintains its original position as shown in Figure 4a. Though the strain breaks the crystal symmetry, the atomic displacement of A_{1g} mode is perpendicular to the atomic plane and the strain has little effect on the A_{1g} mode. On the contrary, the E_{2g}^1 mode splits into two sub-peaks, the E_{2g}^{1+} and E_{2g}^{1-} as described in literature.[16, 37] The integrated Raman intensity of A_{1g} mode remains unchanged. The total intensity of E_{2g}^1 mode now splits between E_{2g}^{1+} and E_{2g}^{1-} modes. Moreover, these two sub-peaks show obvious red shifts as the strain increases illustrating that the strain-induced symmetry break leads to phonon softening. The peak positions of the E_{2g}^{1+} and E_{2g}^{1-} modes as a function of strain is shown in Figure 4c. The Raman shift rates are obtained by linear fitting. The Raman shift rates of the two sub-peaks are different. The E_{2g}^{1+} mode shifts by $-1.01 \pm 0.46\ cm^{-1}/\%$ strain, while the E_{2g}^{1-} mode shift by a larger rate of $-6.3 \pm 0.74\ cm^{-1}/\%\ strain$. There is no obvious hysteresis between the strain loading and unloading processes proving that no slippage between the MoS_2 and the PET substrate.

Figure 4b shows the evolution of C mode on strain. The C mode is relatively less sensitive to strain as compared to the E_{2g}^1 mode. More importantly, a peak splitting (guided by the two black dash dot arrow lines) of the C mode can also be observed. As the strain increases to 0.25%, a small splitting can be observed and the splitting becomes more and more intense when the strain rises up to 0.81%. However, no measurable Raman shift for the LB mode centered at 21.4 cm^{-1} is observed except the gradually reduced integrated Raman intensity as guided by the red dash dot arrow line as shown in Figure 4b.

Unlike the high frequency E_{2g}^1 mode, the two sub-peaks C^+ and C^- modes show opposite variation trends on strain. The C^- mode red shifts before the strain rises up to 0.25% then almost remains at the same position regardless of further increase in strain. In contrast, the C^+ mode shows a gradual blue shift as the strain increases. The peak positions of the C^+ and C^- modes as a function of strain is shown in Figure 4d. The C^+ mode blue shifts for 0.75 cm^{-1} as the applied strain increased to 0.81%, while the C^- mode redshifts by 1.8 cm^{-1}. In the strain range of 0.25-0.81%, the C^- mode almost remains at its original position. This doubly degenerated behavior for C mode may results from the symmetry of lattice vibration. Referring to the E_{2g}^1 mode, the E_{2g}^1 mode involves opposite vibration of two sulfur atoms with respect to the molybdenum atom in plane and the adjacent vibration directions of these atoms are just opposite with each other. Analogously, the E_{2g}^2 mode also consists of opposite vibration between neighboring layers. The two modes belong to the same symmetry.[27] Therefore, the C mode also splits into two sub-peaks under strain. Though the strain induced split of C mode is not as strong as that in the high frequency E_{2g}^1 mode, the small split demonstrates that strain can distort the lattice symmetry in 2D materials and similar behavior can be observed in various phonon vibration modes with the same symmetry. As the mechanism of opposite Raman shifts for C^+ and C^-modes, it may be attribute to the properties difference between the even and odd layer number in the multilayer MoS_2.[32] Further experiments and theoretical calculations are needed to understand the splitting mechanism of the low frequency modes.

Conclusions

In summary, the effect of strain on the shear mode (C mode) and layer breathing mode (LB mode) of few layers MoS_2 was studied comprehensively. Notably, the C mode is also doubly degenerated similar to the E_{2g}^1 mode with respect to the applied strain. Moreover, the two sub-peaks, C^+ and C^- shift oppositely as the strain increases. However, the frequency of LB mode is immune to the uniaxial strain

except its integrated Raman intensity. As the strain increases, the intensity of the LB mode weakens gradually. In addition, the C and LB modes are highly sensitive to the layer number of few layer MoS_2. The evolution of the C mode as a function of layer number can be fitted by a linear-chain model with an additional linear component very well. Our findings pave a path to study the mechanism of low-frequency lattice vibration of various two dimensional layered crystals.

Acknowledgements

This work was financially supported by the PolyU grants (1-ZE14 and 1-ZVGH) and the Research Grants Council (RGC) of Hong Kong (Project no. PolyU 153030/15P).

References

[1] K. F. Mak, C. Lee, J. Hone, J. Shan, T. F. Heinz, *Phys. Rev. Lett.*, 105, 136805 (2010).

[2] R. F. Frindt, *J. Appl. Phys.*, 37, 1928 (1966).

[3] Y. H. Lee, X. Q. Zhang, W. Zhang, M. T. Chang, C. T. Lin, K. D. Chang, Y. C. Yu, J. T. Wang, C. S. Chang, L. J. Li, T. W. Lin, *Adv. Mater.*, 24, 2320 (2012).

[4] B. Radisavljevic, A. Radenovic, J. Brivio, V. Giacometti, A. Kis, *Nat. Nanotechnol.*, 6, 147 (2011).

[5] A. Splendiani, L. Sun, Y. Zhang, T. Li, J. Kim, C. Y. Chim, G. Galli, F. Wang, *Nano Lett.*, 10, 1271 (2010).

[6] B. Radisavljevic, M. B. Whitwick, A. Kis, *ACS Nano*, 5, 9934 (2011).

[7] H. Wang, L. Yu, Y. H. Lee, Y. Shi, A. Hsu, M. L. Chin, L. J. Li, M. Dubey, J. Kong, T. Palacios, *Nano Lett.*, 12, 4674 (2012).

[8] K. S. Novoselov, D. Jiang, F. Schedin, T. J. Booth, V. V. Khotkevich, S. V. Morozov, A. K. Geim, *Proc Natl Acad Sci U S A*, 102, 10451 (2005).

[9] H. Zhang, *ACS Nano*, 9, 9451 (2015).

[10] Z. H. Ni, T. Yu, Y. H. Lu, Y. Y. Wang, Y. P. Feng, Z. X. Shen, *ACS Nano*, 2, 2301 (2008).

[11] P. Lu, X. Wu, W. Guo, X. C. Zeng, *Phys. Chem. Chem. Phys.*, 14, 13035 (2012).

[12] H. Peelaers, C. G. Van de Walle, *Phys. Rev. B*, 86, (2012).

[13] M. Hosseini, M. Elahi, M. Pourfath, D. Esseni, *J. Phys. D: Appl. Phys.*, 48, 375104 (2015).

[14] Y. Wang, C. Cong, C. Qiu, T. Yu, *Small*, 9, 2857 (2013).

[15] K. He, C. Poole, K. F. Mak, J. Shan, *Nano Lett*, 13, 2931 (2013).

[16] H. J. Conley, B. Wang, J. I. Ziegler, R. F. Haglund, Jr., S. T. Pantelides, K. I. Bolotin, *Nano Lett.*, 13, 3626 (2013).

[17] C. Rice, R. J. Young, R. Zan, U. Bangert, D. Wolverson, T. Georgiou, R. Jalil, K. S. Novoselov, *Phys. Rev. B*, 87, 081307(R) (2013).

[18] M. Y. Li, Y. Shi, C. C. Cheng, L. S. Lu, Y. C. Lin, H. L. Tang, M. L. Tsai, C. W. Chu, K. H. Wei, J. H. He, W. H. Chang, K. Suenaga, L. J. Li, *Science*, 349, 524 (2015).

[19] P. H. Tan, W. P. Han, W. J. Zhao, Z. H. Wu, K. Chang, H. Wang, Y. F. Wang, N. Bonini, N. Marzari, N. Pugno, G. Savini, A. Lombardo, A. C. Ferrari, *Nature Mater.*, 11, 294 (2012).

[20] A. Castellanos Gomez, M. Buscema, R. Molenaar, V. Singh, L. Janssen, H. S. J. van der Zant, G. A. Steele, *2D Materials*, 1, 011002 (2014).

[21] T. Mohiuddin, A. Lombardo, R. Nair, A. Bonetti, G. Savini, R. Jalil, N. Bonini, D. Basko, C. Galiotis, N. Marzari, K. Novoselov, A. Geim, A. Ferrari, *Phys. Rev. B*, 79, 205433 (2009).

[22] G. Tsoukleri, J. Parthenios, K. Papagelis, R. Jalil, A. C. Ferrari, A. K. Geim, K. S. Novoselov, C. Galiotis, *Small*, 5, 2397 (2009).

[23] L. Gong, R. J. Young, I. A. Kinloch, I. Riaz, R. Jalil, K. S. Novoselov, *ACS Nano*, 6, 2086 (2012).

[24] A. Castellanos Gomez, R. Roldan, E. Cappelluti, M. Buscema, F. Guinea, H. S. van der Zant, G. A. Steele, *Nano Lett.*, 13, 5361 (2013).

[25] R. J. Young, L. Gong, I. A. Kinloch, I. Riaz, R. Jalil, K. S. Novoselov, *ACS Nano*, 5, 3079 (2011).

[26] C. Lee, H. Yan, L. E. Brus, T. F. Heinz, J. Hone, S. Ryu, *ACS Nano*, 4, 2695 (2010).

[27] J. Verble, T. Wieting, *Phys. Rev. Lett.*, 25, 362 (1970).

[28] T. Li, G. Galli, *J. Phys. Chem. C*, 111, 16192 (2007).

[29] H. Li, Q. Zhang, C. C. R. Yap, B. K. Tay, T. H. T. Edwin, A. Olivier, D. Baillargeat, *Adv. Func. Mater.*, 22, 1385 (2012).

[30] T. J. Wieting, J. L. Verble, *Phys. Rev. B*, 5, 1473 (1972).

[31] H. Zeng, B. Zhu, K. Liu, J. Fan, X. Cui, Q. M. Zhang, *Phys. Rev. B*, 86, 241301(R) (2012).

[32] X. Zhang, W. Han, J. Wu, S. Milana, Y. Lu, Q. Li, A. Ferrari, P. H. Tan, *Phys. Rev. B*, 87, 115431 (2013).

[33] R. Zallen, M. Slade, *Phys. Rev. B*, 9, 1627 (1974).

[34] S. B. Desai, G. Seol, J. S. Kang, H. Fang, C. Battaglia, R. Kapadia, J. W. Ager, J. Guo, A. Javey, *Nano Lett.*, 14, 4592 (2014).

[35] Y. Wang, C. Cong, W. Yang, J. Shang, N. Peimyoo, Y. Chen, J. Kang, J. Wang, W. Huang, T. Yu, *Nano Research*, 8, 2562 (2015).

[36] X. Zhang, X. F. Qiao, W. Shi, J. B. Wu, D. S. Jiang, P. H. Tan, *Chem. Soc. Rev.*, 44, 2757 (2015).

[37] R. Rafael, C. G. Andrés, C. Emmanuele, G. Francisco, *J. Phys.: Condens. Matter*, 27, 313201 (2015).

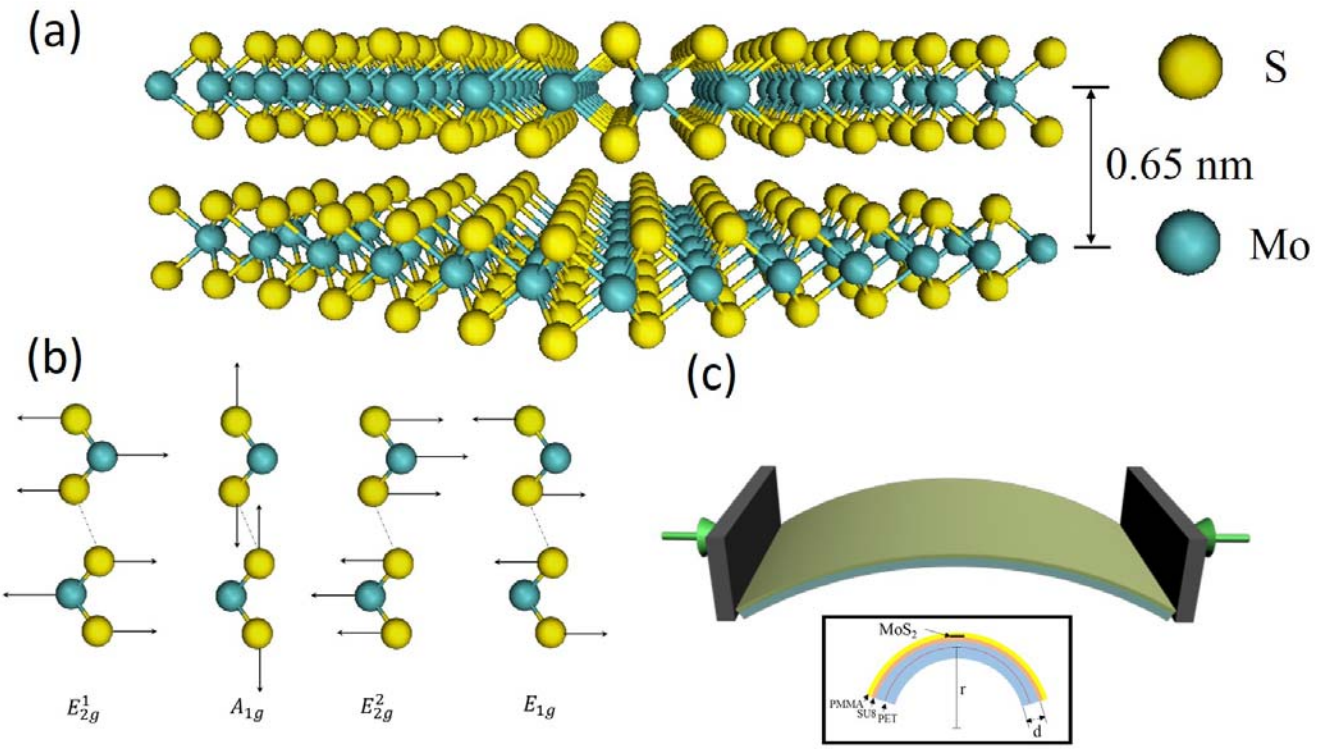

Figure.1 Molecular structures of MoS_2 and the experiment setup. (a) Three dimensional schematic model of the a two-layer MoS_2 structure. The interlayer distance is 0.65 nm. (b) Atomic displacements of the four Raman modes, E_{2g}^1 , A_{1g} , E_{2g}^2 and E_{1g} . (c) Schematic diagram (not to scale) of the experimental setup. Two points bending method is utilized to apply tunable uniaxial tensile strain. The inset shows the cross-sectional view of the PMMA encapsulated few layers MoS_2 on the PET susbtrate. The MoS_2 flake are sandwiched by the bottom SU-8 photoresist layer and the top PMMA layer.

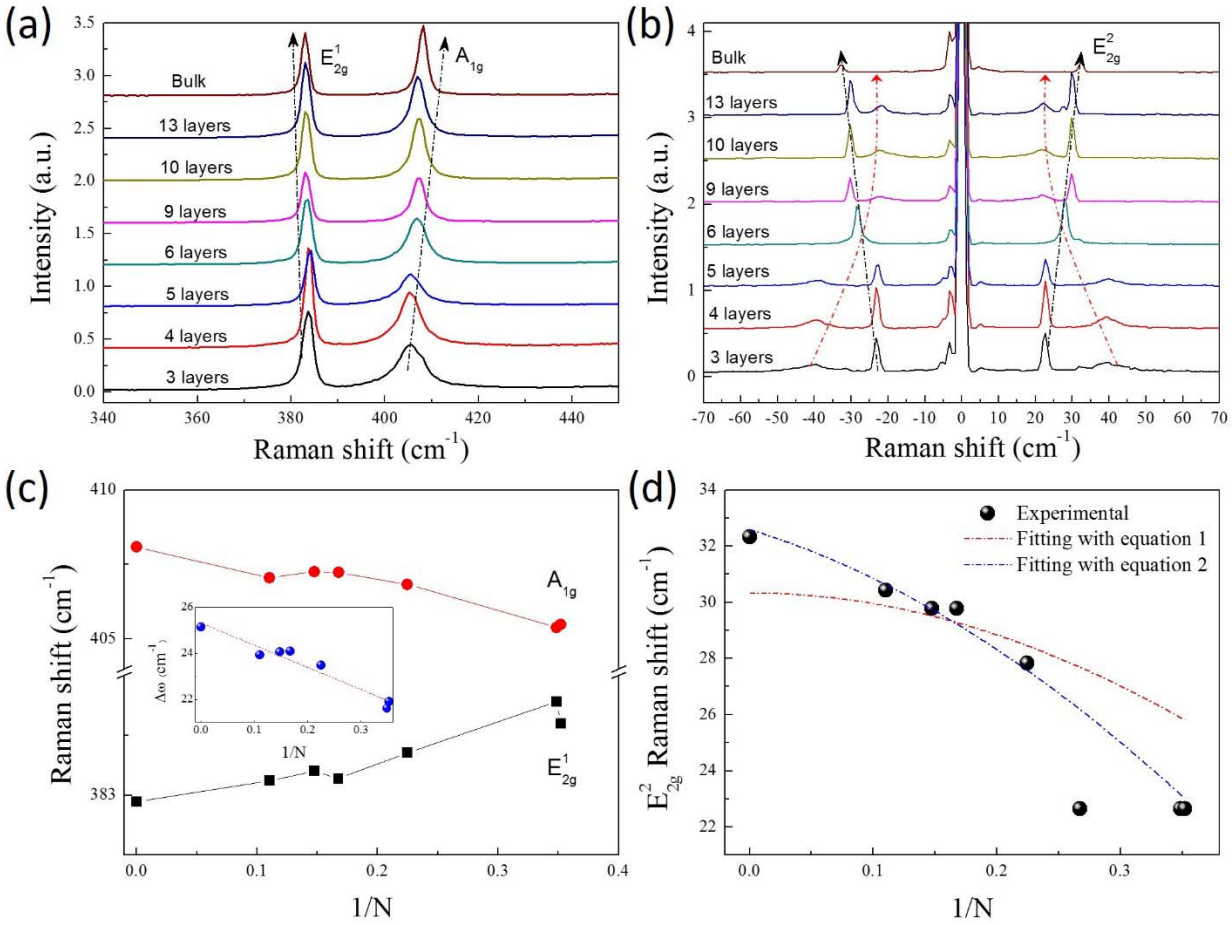

Figure.2 Raman shifts of few layers MoS_2. (a) The evolution of the Raman spectra of the MoS_2 with different layers. The black dash dot arrow lines are the guide of the peak positions. (b) Raman spectra of the C and LB modes as a function of the sample thickness. The black and red dash dot arrow lines represent the C mode and LB mode respectively. (c) The peak positions of the A_{1g} and E^1_{2g} modes as a function of the 1/N. The inset gives the trend of the frequency difference of the two modes as a function of 1/N. (d) Thickness dependence of the Raman shift for the C mode. The black solid dots are experimental values. The red dash dot line is the fitting with the normal linear-chain model. And the blue dash dot line is the fitting with a modified model.

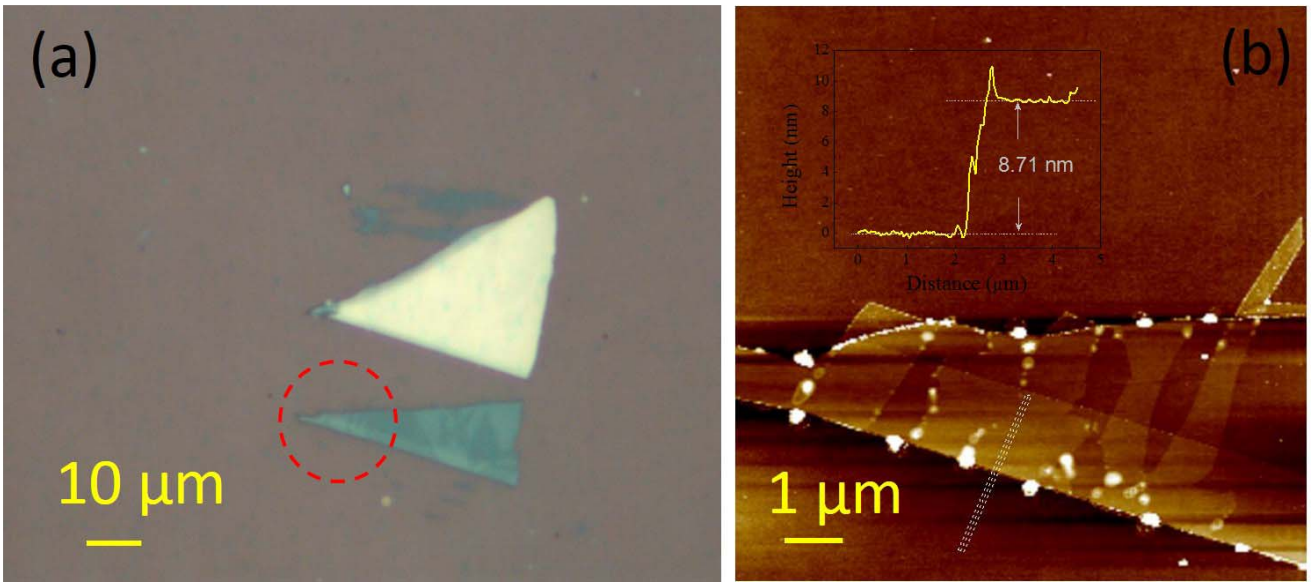

Figure.3 (a) Optical image of the few layers MoS_2 deposited onto the flexible PET substrate. The laser spot is positioned at the red dashed circle. (b) AFM image of the MoS_2 flake. The inset shows the thickness of the sample (8.71 nm).

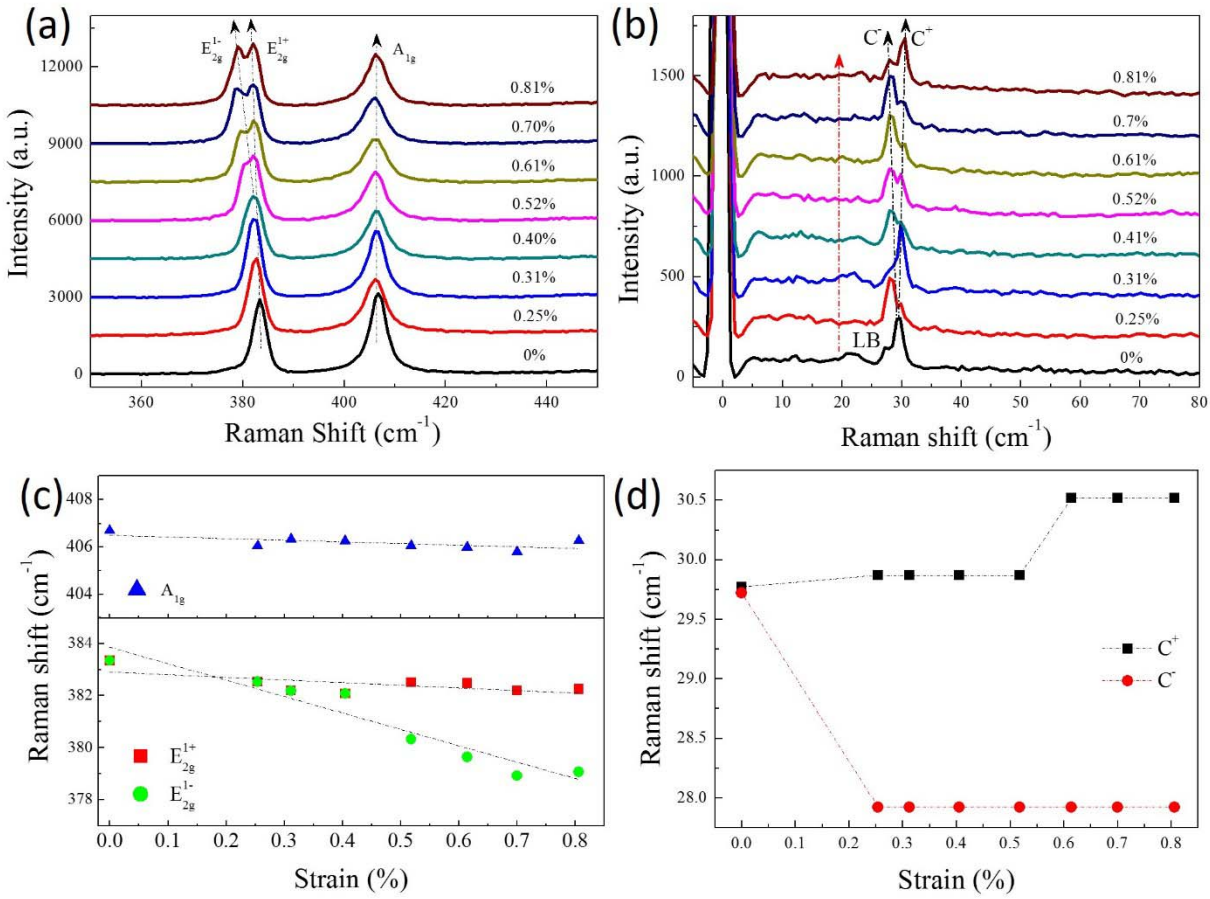

Figure.4 (a) Evolution of the Raman spectra for the E_{2g}^{1} and A_{1g} modes as a function of strain. The variation trends of the peak positions are guided by the black dash dot arrow lines. (b) Evolution of the C and LB modes as a function of strain. The black and red dash dot arrow lines represent C mode and LB mode, respectively. (c) Strain dependence of the peak positons of E_{2g}^{1+} , E_{2g}^{1-} (lower panel) and A_{1g} modes (upper panel). The black dash dot lines are linear fitting. (d) The peak positions of the divisive C^{+} and C^{-}modes as a function of strain.